13th International Conference on Computer and Knowledge Engineering (ICCKE 2023), November 1-2, 2023, Ferdowsi University of Mashhad, Iran

Computational Microscopy Based on Fourier Ptychography using Embedded Architecture

Rezvan Mir
Dept. of Computer Engineering
Ferdowsi University of Mashhad
Mashhad, Iran
Email: mir.rezvan@mail.um.ac.ir

Abedin Vahedian
Dept. of Computer Engineering
Ferdowsi University of Mashhad
Mashhad, Iran
Email: vahedian@um.ac.ir

***Abstract*—Conventional imaging systems demonstrate a clear trade-off between resolution and field-of-view in acquired images. This review discusses a new method called Fourier Ptychography (FP), which leverages super-resolution to overcome this trade-off in image generation. Specifically, FP sequentially captures low-resolution images under different illumination angles and stitches them in the frequency domain. The variety of angles enables access to multiple frequency regions. This method can be implemented on simple microscopes with an exchange of optical design complexity for computational complexity to achieve high-quality imaging. This paper demonstrates how to use FP in a fast, robust, and low-cost manner. An experimental model using an embedded system, namely *Raspberry Pi 4*, a low-cost microscope, is proposed to achieve super-resolution enhancement and wide-field imaging with sub-micron resolution. This microscopy can be assembled using a collection of readily available parts.**

***Index Terms*—Fourier Ptychography, embedded system, super-resolution enhancement, sub-micron resolution**

I. Introduction

The optical microscope has been a valuable tool for biological and biomedical imaging applications and often requires high-resolution images to observe cellular structures or large tissue areas. Achieving high-resolution imaging and visualizing subcellular structures, that indicate the cell condition requires the use of a high-magnification lens. However, high-resolution imaging is an expensive method and may not always be available due to lens limitations. Zoom-in features limit the accessibility of observation specimen area and overall tissue, and often it creates limitations for what we were looking for. Ideally, an imaging system should desire to provide high-resolution and a broad Field Of View (*FOV*) concurrently. Conventional cameras and microscopes can either achieve high-resolution image zoom-in or zoom out a larger area with lower resolution, but these rarely happen at the same time.

In customary imaging, the number of pixels in the detector array is an important limitation [1], so increased FOV can become only at the expense of reduced spatial resolution. The spatial bandwidth product (*SBP*) can be interpreted as the efficient information channel bandwidth for collecting data from images in the physical system. The purpose is to achieve high SBP in microscopy. An approach for increasing the SBP of microscopy is to use larger detector arrays accompanied by higher performance optics, which unfortunately leads to increased aberrations and complexity [2].

Recently, a new method called Fourier Ptychography Microscopy (*FPM*) has been developed to improve the resolution of imaging systems. It is a computational imaging technique that achieves high-resolution throughout the entire image using a low numerical aperture (*NA*) lens and a large FOV, as a result, to obtain gigapixel images [3]. The key to understanding FP lies in Fourier Transform (*FT*). By describing the optical properties of a sample, high-frequency components of FT can be considered as fine details of the sample, and low-frequency components as large-scale spatial features.

When an object is illuminated by parallel beams of light, a lens placed at a focal distance will form certain light patterns at the back focal plane. In the Fourier plane, the spatial allocation of the light corresponds to the FT of the desired sample, usually known as its Fourier spectrum. One of the key purposes of designing high-resolution microscopes is to create an ample Fourier space that passes a widespread scope of spatial frequency spectra.

In FP, spectrum scanning is performed in the Fourier domain, and the acquired image is in the spatial domain. This is achieved using a programmable LED array and angle-shifting of the illumination wavefront. According to studies, this technique has been able to computationally: I) improve SBP, II) eliminate optical aberrations or distortions, III) retrieve pupil functions throughout the sample, and IV) retrieve phase information solely from intensity images. In addition to providing all the advantages of Real-space ptychography, the FP imaging system can be constructed using low-cost components [4]. Unlike Real-space ptychography, FP does not

979-8-3503-3015-1/23/$31.00

require a high-coherence light source or a detector with a high dynamic range and moving parts. This makes it an ideal choice for applications where cost is a major concern.

FP can be implemented in moveable and turnkey systems. So far, various attempts have been made to use embedded systems and adapt them to a simple optical configuration. Several ptychography-based microscopes have been reported: a portable high-resolution FPM using a smartphone lens [5], a low-cost FPM-based on *Raspberry Pi* hardware with sub-micron resolution [6], a low-cost platform for creating high-quality moldless lenses [7], and finally, a microscope that can be installed on a smartphone and use its display screen as a programmable illumination [8]. It should be noted that most of the above processing is still carried out on the server.

In terms of experimental implementation, FP is a simple and widely used technique that can achieve gigapixel images in both amplitude and phase domains. It also has the capability of quantitative phase reconstruction and removal of optical aberrations at a low cost. The main limitation of the FPM technique is convergence to a local optimum solution and its sensitivity to noise. Noise can distort high-frequency information in the image and affect the quality of the reconstructed image. In this paper, we report the implementation of a low-cost and high-resolution FPM using a *Raspberry Pi* computer for data acquisition and improving image quality.

The structure of the manuscript is organized as follows. In part II, we acquaint the general principle of FP and propose an algorithm for improvement. Part III discusses the proposed method's implementation and the introduction of hardware and its software components. In part IV, we compare the experimental setup and experimental results for the proposed system. Eventually, in part V, discussions and conclusions are summarized.

II. Principles And Methods

A. Principle Of FPM

The basic operation of FP imaging is represented in Figure 1. When a sample is illuminated by a moving point-like source of light waves, spatial patterns of light are formed at different angles of illumination on a specific plane behind a lens. These point-like sources of light are illuminated time-sequentially, capturing an image at per angle. Only a tiny portion of this Fourier spectrum may pass through the imaging system and reach the sensor image due to the size limitation of the objective lens. Therefore, the effect of the lens on the diffraction spectrum can be considered a low-pass filter, allowing a narrow aperture of frequencies to pass through in the Fourier domain (pupil function) and filtering out higher frequencies. When an object is illuminated with a plane wave at higher angles, scattered light from the sample is represented as a Fourier spectrum. In some cases, this scattered light does not pass through the NA of the lens, creating a limitation for the imaging system's resolution. Illuminating the sample with different angles enables access to more spectra and aids in the appearance of the image. In other words, the basic principle of FP is to take a number of low-resolution images using lenses with a low-NA objective at different illumination angles and then try to combine the different information in those images and improve the final image resolution.

In the overall framework of FPM, the sample image is captured under different illumination angles using an array of LEDs. Each image is divided into multiple sub-regions for processing as illumination angles vary for different sub-regions. Nine unique windows of the specimen's Fourier spectrum have been shown here. By acquiring unique images at different angles, FP captures many regions of FT components covering a wide spectrum. Achieving this wide range is done by acquiring low-resolution images in the Fourier domain and stitching them together. Thus, when the final image is reconstructed, it will fix features with higher resolution.

What happens is that, by scanning the angle of illumination, we essentially get to scan the angular spectrum of the transmitted light through the sample around the imaging system. That is equivalent to rotating the lens around to collect multiple images over the very vast angular range of the imaging equipment. So, combining that information effectively works by increasing the effective NA of the imaging system, and that's why the final resolution is getting better.

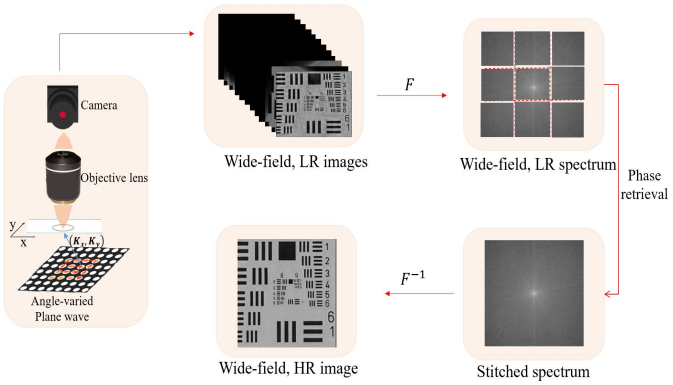

Fig. 1: Basic operation of FP.

B. Reconstruction Method

The Fourier ptychographic reconstruction process involves integrating several low-resolution measurements to recover the wavefront phase at full-field high-resolution. This results in increased resolution compared to a conventional microscope. Such synthesis relies on phase information that may be lost during the data acquisition process. Therefore, in order to recover the frequency spectrum of the image with high-resolution, we need to know its phase. Inverse mathematical operations cannot be carried out without knowing the phase information. In other words, a light wave's propagation through a sample delays it by a certain amount, which is described by phase information. Applying phase recovery concepts, FP leverages the Gerchberg-Saxton-Fienup (*GSF*) algorithm's iterative reconstruction technique to recover the sample's lost phase information [9]. The constraint of

what is known in both the real and mutual space domains is fulfilled by the iteration between the object and Fourier domains. In order to obtain the correct diffraction patterns in the mutual space, the object is laterally translated in a probe beam that is constrained in the real space. Two distinct sets of constraints are imposed on the reconstruction process iteratively. The limited probe's beam acts as a compact support constraint in real space, limiting the object's physical extent for each measurement. The estimated solution in the mutual space is based on the diffraction data, which also function as limitations on the Fourier magnitude. The iterative reconstruction process effectively seeks an estimation of the object that satisfies both constraints [10]. The GSF algorithm is designed to reconstruct complex wave field in a general situation. The phase is obtained from intensity measurements taken at different levels, and the amplitudes are assumed to be known in both the object and Fourier domains.

Various studies have been conducted to improve FPM image reconstruction and minimize the impact of noise. These studies can be categorized into two sections: Section 1 offers a pre-processing of the FP's raw dataset. In the FP imaging process, the input low-resolution images have a relatively low signal-to-noise ratio; Hence, applying methods to reduce noise in the raw FPM dataset is essential. Image pre-processing enables the automatic selection of affected images from the raw dataset and then removes their adverse effects in the reconstruction process. Noise reduction methods based on pre-processing have been explored in [11] and [12].

Section 2 comprises algorithms that have been proposed to converge to a local optimum. The main goal of these algorithms is first to identify different types of noise and then search for an optimal solution to minimize it. This approach optimizes the phase-retrieved solution based on a gradient descent scheme. Subsequently, optimized results are searched using a weighted item and, at each step, the suppression of noise is pursued using these measures. This process leads to an improvement in the quality of high-resolution reconstructed images. The proposed methods based on improving convergence are mentioned in [13], [14], and [15]. The method presented in this paper is based on a reconstruction algorithm to improve convergence, which is implemented on FPM; We will discuss it in detail in the following section.

III. FPM System Implementation

FPM still requires considerable time to achieve a high-resolution image with a broad FOV while working with volume data of low-resolution images. An optimization strategy that uses incremental gradient descent is the Adaptive Step-size (*AS*) algorithm [15]. In this method, all FT is not processed. Incremental methods are based on the alternating projection of the probe and object functions on the measurement plane and iteratively update the probe and object functions until convergence. Using the AS algorithm on FP significantly reduces the time and effectually improves the quality of the reconstructed image and the robustness to noise.

The image foundation process in FP is defined as equation 1, which describes the problem of diffracted wave propagation. The FT operation is applied to the product of the pupil transfer function (A(k)) in the frequency spectrum of a given object shifted S(k) by the illumination angles in the spatial domain.

$$I_i(r) = FT\left[A(K) \times S(K - K_i)\right](r) \tag{1}$$

Initially, the reconstruction process in FP is that an estimate of the spatial frequencies of the $S(K)$ object is made with high-resolution. Then, using the supplied shift variable illumination angle i and the filtered pupil function A, we generate $S_i(K - K_i)$. In the next step, the generated $S_i(K - K_i)$ is propagated to the detector plane to produce an approximate representation of the image formed on the detector. The reported intensity image $I_i(r)$ is used to calculate the amplitude of this approximation. Finally, $S_{i-Update}(K - K_i)$ is updated in accordance with equation 2 on the foundation of a gradient descent method, based on the updating of this amplitude and propagating the new image approximation to the object's frequency plane:

$$\begin{aligned} S_{Update}(K - K_i) = S(K - K_i) + \frac{\bar{A}}{|A_{max}|^2} \\ \times \left(S_{i-Update}(K - K_i) - S_i(K - K_i)\right) \end{aligned} \tag{2}$$

To generate a new approximation $S(K)$, we need to go back to $S_{Update}(K - K_i)$ once. So, this is applied to the following illumination angle, and so on, until all illumination angles have been used. The estimated image error, which is the difference between the original and the estimated image, is computed after each iteration. The whole process is repeated if this error exceeds the acceptable limit. Otherwise, the reconstruction process will be aborted. Once the process is complete, an inverse FT is performed on the final $S(K)$ estimate to recover the high-resolution object.

Phase retrieval can be propounded as a regularized optimization problem. So the update function above is optimized as follows:

$$\begin{aligned} S_{Update}(K - K_i) = S(K - K_i) + \alpha \frac{|A|}{|A_{max}|} \frac{\bar{A}}{\left(|A|^2 + \varepsilon\right)} \\ \times \left(S_{i-Update}(K - K_i) - S_i(K - K_i)\right) \end{aligned} \tag{3}$$

In the above Equation, ε is considered as a regularization parameter, and step size α is defined to the update function. Convergence cannot be guaranteed when α is equal to the constant value 1. Therefore, defining it adaptively helps access convergence faster. The step size is reduced whenever there is sufficient progress in image quality is not made. Only a pint-size patch of the object function is updated in each iteration.

Accurate illumination angle estimate and recovery of the spatially variable pupil aberration are prerequisites for a successful FP reconstruction. The estimate of the object and the

Initialization

1. Initialize Sample $S(k)$, Pupil $A(k)$ and k_i

Note: The acquired images $I_i(x,y)$ has an image dimension $m \times n$ of pixels. The fourier spectrum and the final recovered sample have an image dimension of $M \times N$ pixels.

Iterative reconstruction process

2. **for** j^{th} iteration **do**
3. **for** i^{th} illumination **do**
4. Create a cropped a subregion and shifted spectrum:k_{xi}, k_{yi} :

$$S_{\text{crop}}(1{:}m, 1{:}n) = S\left(\frac{M-m}{2} + k_{xi} + 1 : \frac{M+m}{2} + k_{xi}, \frac{N-n}{2} + k_{yi} + 1 : \frac{N+n}{2} + k_{yi}\right)$$

5. Compute estimated exitwave: $\Psi_i'(k_x, k_y) = S_{\text{crop}}(k_x, k_y) \times A(k_x, k_y)$ #Low-pass Filtering
6. Propagate to Fourier domain: $\psi_i'(x,y) = I\mathcal{FT}[\Psi_i'(k_x, k_y)]$ #generate the low-resolution images
7. Spatial domain optimization (replace the amplitude and keep the phase unchanged)
8. Propagate to spatial domain: $\Psi_i'(k_x, k_y) = \mathcal{FT}[\psi_i'(x,y)]$
9. Update the non-cropped spectrum using the rPIE algorithm:

$$S_{Update}(K - K_i) = S_{\text{crop}}(K - K_i) + \frac{\bar{A}}{(1-\alpha)|A|^2 + \alpha|A_{max}|^2}\left(S_{i\_Update}(K - K_i) - S_i(K - K_i)\right)$$

10. **end for**
11. **end for**

Fig. 2: FPM reconstruction and optimization process algorithm.

pupil function are initialized for reconstruction at the beginning. Raw intensity measurements can give a decent initial estimation of the object being reconstructed in experimentally acquired images since they contain low-frequency information. The estimated initial frequency spectrum is generated by the FT of the spatial domain with high-resolution as a result of doing the reconstruction in the Fourier domain. Through the coherent transfer function, the pupil function $A(K)$ is initialized. For each K_i illumination, the sampling vectors are computed in 2D coordinates. The purpose of this reconstruction is the synthesis of the measurements in the Fourier domain to recover the frequency spectrum $S(K)$. Through propagation from the Fourier domain to the spatial domain, the high-resolution object $S(r) = IFT\{S(K)\}$ can be obtained (spatial domain coordinates are what the r parameter denotes). Figure 2's algorithm shows how to combine measurements and constraints. An iterative approach is used to update the object and the pupil until it finally converges to a solution. Updates to $S(K)$ and $A(K)$ are made using all illumination angles, or a subset of them, in each iteration. The updating is done in two spatial and Fourier domains.

Figure 3 shows an arrangement. The microscope uses a *Raspberry-Pi 4* single-board as an embedded system for data acquisition, controlling the camera, and the illumination of LEDs, enabling imaging and data transfer without the need for a peripheral system. Other required hardware for this is an LED array, camera, and lens in addition to the *Raspberry-Pi* board.

The main hardware and software control parts of the microscope are shown in Figure 4. Firstly, the LED array is lit according to the program given to it, then to perform the imaging the camera is accessed and controlled by Python 3.8 programming language. Images with a Python script using the NumPy library are pre-processed with a raw data format on *Raspberry-Pi*. Finally, the pre-processed raw images are stored

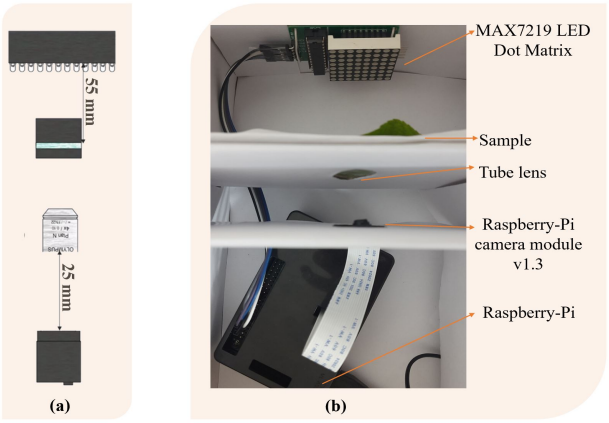

Fig. 3: a) Proposed Kit model and (b) A setup of the assembled microscope.

in the SD card memory.

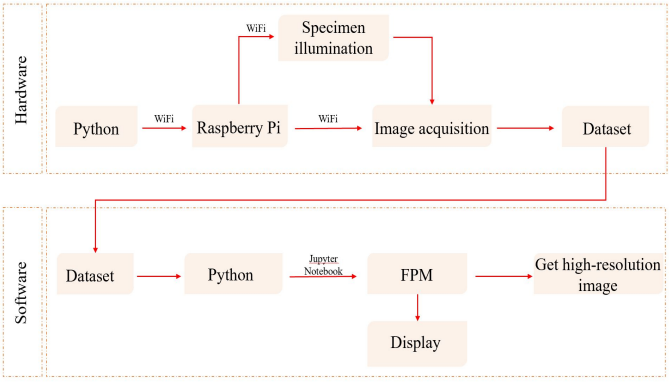

Fig. 4: Hardware system and control of software of FPM.

The stored images are split into 512×512 pixel sub-images with 8 pixel overlap to aid high-resolution reconstruction stitching. In the next step, the sub-images are transferred to the Jupyter Notebook processing package in the Python programming language for further pre-processing and are processed by the SciPy, OpenCV, and Pillow libraries.

IV. Experiment

A. Experimental Setup

The dimensions of the microscope are *7cm* × *11cm* × *8cm* and it weighs only *160 grams*. The *Raspberry-Pi 4* enables data transfer and wireless image acquisition. The light source used in this implementation is an off-the-shelf LED array with a matrix of 8×8 and a pitch of 4mm, which is lit up sequentially. The LED illumination patterns are controlled by the *Raspberry-Pi*. The distance between the LED array and the specimen is 55 mm, and the pixel size of the camera is 1.4 µm with a magnification of 8.15. The coordinates for the first LED are set to X = 0, Y = 0. Images were acquired using a *Raspberry-Pi* camera module and saved in tiff

format. After capture, the images were converted to grayscale. The *Raspberry-Pi* is used to control the LED illumination patterns. The camera has a 1.4 µm pixel size and an 8.15x magnification, and the distance between the LED array and the specimen is 55 mm. The coordinates for the first LED are set to X = 0, Y = 0. A *Raspberry-Pi* camera module was used to acquire the images and save them in tiff format. The images were converted to grayscale after they were captured. All materials and their values are detailed in Table I.

TABLE I. FPM design parameters

Mass-produced components	Name	Values
Single board	Model	Raspberry-Pi 4
Camera	Model	Raspberry-Pi camera module v1.3
	Pixel size	1.4 µm × 1.4 µm
Objective Lens	Numerical aperture	0.55
	Sensor resolution	2592 × 1944 pixels
	Optical size	1/4”
Tube Lens	Focal length	120 mm
LED	Model	MAX7219 LED Dot Matrix
	Size module	32 mm × 32 mm × 13 mm
	Pitch	4mm
	Wavelength	625 ∼ 630 nm

B. Experimental Results

In this experiment, 64 low-resolution images were taken to restore one high-resolution snapshot. The recovery process changes between the spatial (captured intensity images) and frequency domains. In the spatial domain, low-resolution images are used to limit the amplitude of the solution, and in the Fourier domain, a pupil function is applied to the solution as a constraint. This constraint is shifted in the Fourier domain to reflect different illumination angles.

At the moment the probe modulus reaches its maximum value, we modify the object through a new approximation; Other points are modified by the incident probe module. If an update is done at one position of the probe, then the positions of the other probes with the required FOV should also be updated, updating the function of the object sequentially. The entire process of the above part may be repeated 20 times, so for example, 1280 updates for an 8×8 array of the probe positions improve the object estimation. This algorithm is called PIE *(Ptychographic Iterative Engine)*. The ePIE *(extend PIE)* and rPIE *(regularized PIE)* algorithms are among the algorithms inspired by PIE. These algorithms have been extended to dissolve probe.

The results of reconstruction using the incremental gradient descent searching algorithm are shown in Figure 5. After each algorithm iteration, we calculated the total difference between the evolving object reconstructions and the original raw image. We also stopped the algorithm at various time points to obtain snapshots of the phase reconstruction. Iterating the algorithm corrects for errors caused by component misalignment and spatial aberration that depend on image quality.

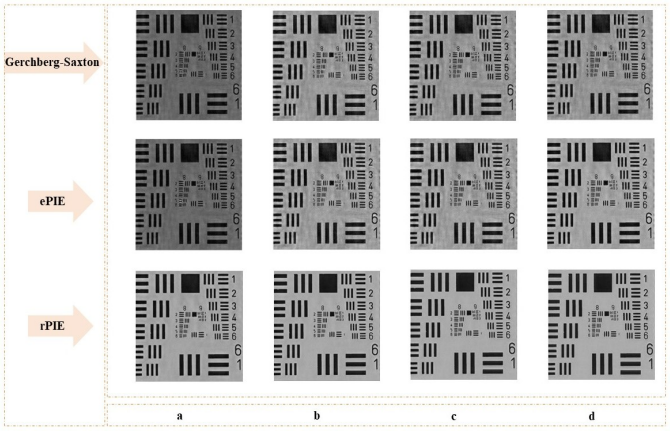

Fig. 5: Progress of reconstructions (a-d) using the recovery algorithm in the proposed method. Image reconstruction using (Top) GSF algorithm, (Middle) ePIE algorithm, and (Bottom) rPIE algorithm.

As shown in Figure 5, the image quality of FP reconstruction using the incremental gradient descent algorithm is superior to the GSF algorithm. Using these algorithms, the central parts are obtained very quickly, whereas the edge reconstruction takes a long time. With ePIE, the outer part takes longer to appear more accurately, but the center of regeneration evolves very quickly. Also, rPIE converges much faster than ePIE at the center and edges.

TABLE II. Parameters obtained from the ePIE’s algorithm.

Parameter	a	b	c	d
PSNR(dB)	104.7128	102.92	102.4138	102.0809
SSIM	0.999	0.998	0.998	0.998
Running time	26.9s	45.1s	55.9s	1m17s
iteration	1	3	5	8

TABLE III. Parameters obtained from the rPIE’s algorithm.

Parameter	a	b	c	d
Alpha	0.25	0.125	0.0625	0.0039
PSNR(dB)	102.0764	101.3394	100.7246	100.2988
SSIM	0.997	0.997	0.997	0.996
Running time	1m51s	2m8s	2m22s	2m38s
iteration	5	7	10	15

Tables II and III indicate the parameters associated with the recovery algorithms. The obtained values in the peak SNR, considering that the image is in grayscale and consists of 8 bits, indicate an acceptable reconstruction between the initial raw image and the final reconstructed image. Criterion SSIM (Structural Similarity Index Method) examines two parameters: luminance masking and contrast masking. The SSIM numbers obtained in this experiment indicate an acceptable level of distortion at the edges of the reconstructed images. Moreover, the use of convergence algorithms significantly reduces the time.

In FPM, significant improvements have been made. Imaging noise is nevertheless a constant issue that can taint the FPM-retrieved data. Without pre-processing the image, the quality of the rebuilt image cannot be improved. With the use of a two-dimensional Gaussian filter, we were able to lower the noise to manageable levels. Figure 6 shows the results of the reconstruction image enhancement.

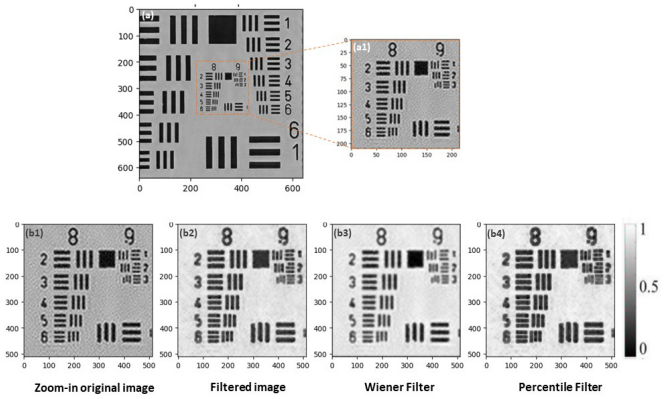

Fig. 6: Improvement results using 2D filtering. (a) The image was captured using an objective lens with 4× magnification and 0.1 NA. (a1) Displays an enlarged image of a specific area within the larger image (a). (b1)-(b4) Results of improving image quality by Gaussian filters.

V. Conclusion

This paper proposes a portable and low-cost microscope using the Fourier ptychography technique implemented on an embedded system. Making high-performance microscopes at a very low-cost is one of the appealing features of FPM. Compared to previous reports on systems equipped with expensive cameras, the microscope offers a 100-fold larger FOV without loss of resolution. In this implementation, data acquisition is done independently and, the data is processed through Jupyter Notebook. We have shown that FPM can be built with accessible mass-produced components. Also, the AS optimization strategy is suggested for utilization in large datasets because of its faster convergence, computational efficiency, and low memory cost. This method eliminates noise more effectively while preserving useful information. Since the quality of the acquired images is outstandingly improved, this proposed microscope can be used for applications such as cell studies. All processing in our work is carried out on the *Raspberry-Pi* board and does not need a server.

Acknowledgements

The USAF dataset we used is open-sourced by Cao Zuo et al. [15].

References

[1] D. Mendlovic, A. W. Lohmann, and Z. Zalevsky, "Space–bandwidth product adaptation and its application to superresolution: examples," *J. Opt. Soc. Am. A*, vol. 14, no. 3, p. 563, 1997.

[2] G. Zheng, C. Shen, S. Jiang, P. Song, and C. Yang, "Concept, implementations and applications of Fourier ptychography," *Nature Reviews Physics*, vol. 3, no. 3. pp. 207–223, 2021.

[3] T. Wang et al., "Optical ptychography for biomedical imaging: recent progress and future directions," *Biomedical. Opt. Express*, vol. 14, no. 2, p. 489, 2023.

[4] P. C. Konda, T. Aidukas, and A. R. Harvey, "Miniature Fourier ptychography microscope using Raspberry Pi camera and hardware," *Opt. InfoBase Conf. Pap.*, no. August, pp. 26–29, 2017.

[5] S. Dong, K. Guo, P. Nanda, R. Shiradkar, and G. Zheng, "FPscope: a field-portable high-resolution microscope using a cellphone lens," *Biomed. Opt. Express*, 2014.

[6] T. Aidukas, R. Eckert, A. R. Harvey, L. Waller, and P. C. Konda, "Low-cost, sub-micron resolution, wide-field computational microscopy using opensource hardware," *Sci. Rep.*, 2019.

[7] T. Kamal, L. Yang, and W. M. Lee, "In situ retrieval and correction of aberrations in moldless lenses using Fourier ptychography," *Opt. Express*, vol. 26, no. 3, p. 2708, 2018.

[8] K. C. Lee, K. Lee, J. Jung, S. H. Lee, D. Kim, and S. A. Lee, "A Smartphone-Based Fourier Ptychographic Microscope Using the Display Screen for Illumination," *ACS Photonics*, vol. 8, no. 5, pp. 1307–1315, 2021.

[9] J. R. Fienup, "Reconstruction of a complex-valued object from the modulus of its Fourier transform using a support constraint," *J. Opt. Soc. Am. A*, vol. 4, no. 1, p. 118, 1987.

[10] S . Jiang, et al., "Spatial-and Fourier-domain ptychography for high-throughput bio-imaging," *Nature Protocols.*,pp. 1-33, 2023.

[11] L. Hou, H. Wang, J. Wang, and M. Xu, "Background-noise reduction for Fourier ptychographic microscopy based on an improved thresholding method," *Curr. Opt. Photonics* 2(2), 165–171 ,2018.

[12] Y. Zhang, A. Pan, and M. Lei, "Data preprocessing methods for robust Fourier ptychographic microscopy," *Opt. Eng.*, vol. 56, no. 12, 2017.

[13] S. Chen, T. Xu, J. Zhang, X. Wang, and Y. Zhang, "Optimized Denoising Method for Fourier Ptychographic Microscopy Based on Wirtinger Flow," *IEEE Photonics J.*, 2019.

[14] L. Bian et al., "Fourier ptychographic reconstruction using Poisson maximum likelihood and truncated Wirtinger gradient," *Sci. Rep.*, vol. 6, no. June, pp. 1–10, 2016.

[15] C. Zuo, J. Sun, Q. Chen, "Adaptive step-size strategy for noise-robust Fourier ptychographic microscopy," *Opt. Express*, 2016, vol. 24,18.